TELLUS

Evaluation of several different planetary boundary layer schemes within a single model, a unified model and a multimodel superensemble

By T. N. KRISHNAMURTI[1]*, S. BASU[2], J. SANJAY[3] and C. GNANASEELAN[1,3],   [1]*Department of Meteorology, Florida State University, Tallahassee, FL 32306, USA;* [2]*Natonal Centre of Medium Range Weather Forecast, Noida, India,* [3]*Indian Institute of Tropical Meteorology, Pune-411008, India*

ABSTRACT

This paper addresses the forecasts of latent heat fluxes from five different formulations of the planetary boundary layer (PBL). Different formulations are deployed within the Florida State University global spectral model. Hundreds of short range forecast experiments are carried out using daily data sets for summer 2002 with each model. The primary goal of this study is to compare the performance of the diverse family of PBL algorithms for the latent heat fluxes within the PBL. Benchmark fluxes are calculated from the vertical integrals of Yanai's formulation of the apparent moisture sink and a precipitation using Physical Initialization. This provides indirectly observed estimates of the vertical fluxes of latent heat in the PBL. This comparison reveals that no single scheme shows a global spread of improvement over other models for forecasts of latent heat fluxes in the PBL. Among these diverse models the turbulent kinetic energy based closure provides somewhat better results. The construction of a multimodel superensemble provides a synthesis of these different PBL formulations and shows improved forecasts of the surface fluxes. A single unified model utilizing weighted PBL algorithms where all the five schemes are retained within a single model shows some promise for improving a single model.

1. Introduction

The modelling of the planetary boundary layer (PBL) fluxes for heat, moisture and momentum carry many uncertainties. Validation of such model fluxes often requires the design of field experiments. Conventional weather observations do not meet the needed information for such validation. Indirectly one can obtain somewhat useful measures of fluxes from the reanalysis data sets by invoking rain rate initialization and performing vertical integrals of the Yanai et al. (1973) apparent heat source and moisture sink computations to arrive at some consistent measures of PBL fluxes. These fluxes are consistent in the sense that they have seen the best estimates of observed rain rates and also the entire tropospheric analysed data sets for winds and moisture. This alternative measure of observed fluxes is used in our study.

Several formulations of the PBLs are currently in use in different Numerical Weather Prediction (NWP) and climate models. In the present study, we shall examine the relative performances of as many as five local and non-local closure schemes based

on K-theory and turbulent kinetic energy (TKE) closures. Given observed estimates of the aforementioned benchmark fluxes it is possible to examine the geographical distribution of differences and systematic errors for these different formulations of the PBL.

Construction of a unified model (that carries several different physical parametrization schemes) has been examined in some detail previously in two of our recent studies. Krishnamurti and Sanjay (2003) examined this approach using six different cumulus parametrization schemes. A single Florida State University (FSU) global spectral model at a high resolution was first run (during a training phase) to carry out some 100 forecasts using each of the six cumulus parametrization schemes. Those showed a varied behaviour for the different schemes, some demonstrating improved skills over others on certain days and certain regions. A multimodel superensemble (Krishnamurti et al., 1999, 2000b) utilized these 600 forecasts and developed a performance statistics for each model based on the observational benchmarks (such as satellite based precipitation estimates). A statistics during a training phase of the superensemble was obtained for a multiple regression utilizing a least-square minimization of model outputs against the observational estimates. Those statistical weights were derived at each geographical location, at each vertical, for each of the variables and for each of the member models. That

*Corresponding author.
e-mail: tnk@io.met.fsu.edu

provided as many as 10^7 statistical weights. These weights were next used to construct superensemble forecasts from the forecasts of member models. In Krishnamurti and Sanjay (2003), a unified model was constructed, where a single forecast model carried the weighted sum of all of these six cumulus parametrization schemes. The performance of the member models, the unified model and the multimodel superensemble were next examined. It was concluded from that study that the unified model did better in terms of standard skill scores compared to all member models, however the multimodel superensemble carried the highest skills for the precipitation forecasts.

This same type of a multimodel exercise was also carried out with multiple parametrizations of cloud radiative transfer, Chakraborty et al. (2006). Those studies were aimed at improving the phase and amplitude of the diurnal change for precipitation and clouds out to day 5 of forecasts. We found rather similar results from this hierarchy of experiments. The multimodel superensemble captured the phase and amplitudes of the diurnal change globally out to day 5 of forecasts. The unified model had the next best skill and it outperformed each of the member models in terms of skills. Data uncertainties generally call for ensemble of forecasts. Forecast uncertainties arising from physical parametrization can also be examined in the same context. The present paper explores the ensemble spreads that arise from the use of five different PBL formulations. A unified PBL model and the multimodel superensemble are also examined here.

2. Various PBL schemes used in the FSU model

In the present work, the Florida State University Global Spectral Model (FSUGSM), T170L27, Krishnamurti et al. (1998) is a centrepiece. In this model the vertical eddy fluxes of momentum, heat and moisture are modelled as diffusive fluxes and are expressed by

$$\frac{\partial \tau}{\partial t} = \frac{g^2}{P_s^2} \frac{\partial}{\partial \sigma} \left(\rho^2 K \frac{\partial \tau}{\partial \sigma} \right), \tag{1}$$

where ρ is the air density, K is the eddy diffusivity and $\tau = u$, v, q, or θ. The discretization requires boundary conditions on the flux of τ at the top and bottom of the model atmosphere. Typically, the flux is set to zero at the top boundary and set equal to the surface flux at the bottom boundary. In a first order closure approach the vertical kinematic flux of a quantity is considered proportional to the local gradient of the transported quantity, that is, $\overline{w'\tau'} = -K \frac{\partial \tau}{\partial z}$. Thus the differences in the PBL schemes will depend on the specification of K. A large variety of empirical formulations for K that are based on experimental data can be found in literature (e.g. Blackadar, 1979; Louis, 1979). Within most of these empirical parametrizations, K is usually expressed implicitly in a general form as functions depending on the local vertical wind shear, the parcel mixing length l (which is the av-

erage distance of air (water) parcel turbulent movement towards a reference height and is representative of the local intensity of turbulence), and static stability. K can be also prescribed explicitly as a function of height (e.g. Troen and Mahrt, 1986). These parametrizations usually utilize a fixed shape of the K profile derived from the surface-layer similarity theory close to the ground surface and a certain interpolation formula within the ABL. They are economic and can provide satisfactory results. However, their application is limited to the ABL, whereas the computational domain in NWP models includes the whole troposphere. For at least a half a century it has been accepted that there are regions in the convective PBL where the flux is counter to the local gradient (e.g. Deardorff, 1972; Holtslag and Moeng, 1991). Because countergradient fluxes are thought to be indicative of boundary layer scale eddies, as opposed to small-scale eddies, such fluxes are often called non-local fluxes. A practically sound semiempirical countergradient correction closure for the vertical flux of potential temperature in the convective PBL, and also for fluxes of passive scalars, was developed by Troen and Mahrt (1986). They used the non-local formulation of the fluxes in a K-profile model that diagnoses the PBL depth and then constrains K (the eddy diffusivities or viscosities) to a fixed profile over the depth of the PBL. Variants of the K-profile approach of Troen and Mahrt have since been used in a wide variety of applications, such as climate studies (Holtslag and Boville, 1993), weather forecast models (Hong and Pan, 1996), and mesoscale models. Four such different PBL schemes belonging to the first order closure and also a higher order (one-and-a-half) closure including local as well as non-local schemes were implemented in the FSUGSM.

2.1. Scheme 1 (LBL)

This is a local-K closure approach in which the turbulent mixing is treated by a first order closure. The eddy diffusivity coefficient K ($= K_m$, diffusion for momentum or K_h, diffusion for heat and moisture) is defined as a function of the gradient Richardson number (R_i) (Manobianco, 1988), that is,

$$K = l^2 \left| \frac{\partial \overline{V}}{\partial z} \right| F(R_i). \tag{2}$$

The mixing length l is computed from $l = \dfrac{\kappa z}{1 + \kappa z / \lambda}$, (3)

where $\lambda = 150$ m for momentum and $\lambda = 450$ m for heat and moisture and κ is the von Karman constant (=0.35), Louis (1979). Prandtl surface layer theory and observations showed that $l \cong \kappa z$ close to the surface. Also observations showed that at greater elevations l might not continue to be proportional to distance from ground. The gradient Richardson number for a given atmospheric layer is expressed as $R_i = \dfrac{\frac{g}{\overline{\theta}} \frac{\partial \overline{\theta}}{\partial z}}{\left| \frac{\partial \overline{V}}{\partial z} \right|^2}$. The stability

functions, $F(R_i)$ are of the form

$$
F(R_i) = \begin{cases}
\dfrac{1}{(1+5R_i)^2}, & \text{for stable conditions (Ri} \geq 0) \\[2ex]
\dfrac{1+\alpha\,|R_i|^{1/2}-8R_i}{1+\alpha\,|R_i|^{1/2}}, & \text{for unstable conditions} \\
 & \qquad\qquad (\text{Ri} < 0),
\end{cases} \tag{4}
$$

where α is 1.746 for momentum and 1.286 for heat and moisture (Manobianco, 1988).

2.2. Scheme 2 (FOC)

In this local-K PBL scheme K is determined through mixing length considerations, as discussed above, using semi empirical stability dependent functions based on the bulk Richardson number, R_{ib} (Kanamitsu, 1989; Basu et al., 2002), which is defined as $R_{ib} = \frac{g\,\Delta\theta \times \Delta z}{\theta[(\Delta\overline{U})^2+(\Delta\overline{V})^2]}$. The stability functions $F(R_{ib})$ are of the form

$$
F = \begin{cases}
\dfrac{1}{(1+5R_{ib})^2} & \text{for stable conditions } (R_{ib} \geq 0) \\[2ex]
\dfrac{1+\frac{\alpha}{(\beta)^{1/2}}\,|R_{ib}|^{1/2}+\alpha\,|R_{ib}|}{1+\frac{\alpha}{(\beta)^{1/2}}\,|R_{ib}|^{1/2}} & \text{for unstable conditions} \\
 & \qquad\qquad (R_{ib} < 0),
\end{cases} \tag{5}
$$

where $\alpha = 8$, $\beta = 21$ for momentum and $\alpha = 12$, $\beta = 87$ for heat and moisture (Kanamitsu, 1989).

2.3. Scheme 3 (H&B)

This scheme based on Holtslag and Boville (1993) is a modified gradient (non-local) corrected approach. Here, the fluxes $\overline{(w'\theta')}$ are allowed to flow down the local gradient, an artificial gradient γ is added to the gradient during convective conditions (Holtslag and Moeng, 1991).

Thus $\overline{w'\theta'} = -K(\frac{\partial\bar\theta}{\partial z}-\gamma)$, here, γ reflects the non-local transports due to dry convection $\gamma_c = b\frac{(w'c')_0}{w_s}$, $\overline{(w'c')}_0$ is the corresponding surface flux. Troen and Mahrt (1986) proposed a non-local K closure utilizing K profiles based on O'Brien (1970), in which the eddy diffusivity for momentum, K_{zm} is expressed by $K_{zm} = \kappa w_s z(1-\frac{z}{h})^2$, where h is the boundary layer height defined as

$$
h \cong \frac{\text{Ri}_{cr}[u(h)^2+v(h)^2]}{(g/\theta_s)(\theta_v(h)-\theta_s)}, \tag{6}
$$

where Ri_{cr} is a critical bulk Richardson number for the boundary layer, taken as 0.5, $u(h)$ and $v(h)$ are the horizontal velocity components at h, g/θ_s is the buoyancy parameter, $\theta_v(h)$ is the virtual temperature at h, and θ_s is an appropriate temperature of air near the surface (Troen and Mahrt, 1986). The mixed layer velocity scale $w_s = u_*\phi_m^{-1}$ depends on the surface friction velocity u_*, the surface layer height ($0.1h$) and the Monin Obukhov length L

defined as

$$
L = \frac{-u_*^3}{k(g/\theta_{v0})(\overline{w'\theta_v'})_0}. \tag{7}
$$

The formulation in Holtslag and Boville (1993) differs from that of Troen and Mahrt (1986) in the specification of surface turbulent scales and in the non-local turbulent effects. This was first introduced for climate simulations. The velocity scales w_t for mixing of passive scalars is defined as $w_t = \frac{u_*}{\phi_h}$

For stable [$(\overline{w'\theta_v'})_0 < 0$] (or the surface virtual heat flux is negative) and neutral surface conditions [$(\overline{w'\theta_v'})_0 = 0$],

$$
\phi_h = \begin{cases}
1+5\frac{z}{L} & \text{for} \quad 0 \leq z/L \leq 1 \\
5+\frac{z}{L} & \text{for} \quad z/L > 1.
\end{cases} \tag{8}
$$

The Monin–Obukhov length is often used to characterize the stability of the layer (i.e. $L < 0$ in unstable conditions with upward heat fluxes, $L > 0$ in stable conditions with downward heat fluxes). In stable conditions the exchange coefficients for both heat and momentum are often found to be similar and so it is considered that the velocity scale for winds $w_m = w_t$. For unstable conditions $[(\overline{w'\theta_v'})_0 > 0]$,

$$
\phi_h = \left(1-15\frac{z}{L}\right)^{-1/2},
$$

and

$$
w_m = \frac{u_*}{\phi_m},
$$

where

$$
\phi_m = \left(1-15\frac{z}{L}\right)^{-1/3}. \tag{9}
$$

2.4. Scheme 4 (H&P)

A similar non-local PBL scheme was introduced by Hong and Pan (1996), which is a simplified variant used later for weather prediction.

For the unstable conditions $\phi_m = \left(1-16\frac{0.1h}{L}\right)^{-1/4}$ (10)

Similarly for temperature and humidity $\phi_t = \left(1-16\frac{0.1h}{L}\right)^{-1/2}$ (11)

while for the stable and neutral regimes $\phi_m = \phi_t$

$$
= \left(1+5\frac{0.1h}{L}\right). \tag{12}
$$

2.5. Scheme 5 (TKE)

An improvement to the first-order closure was achieved by introducing more of physics of the atmosphere (within the purview of computational infrastructure) with prognostic equations for the TKE, E and the turbulent dissipation, ϵ. This approach is called $E - \epsilon$ closure, in which knowing the E, ϵ as well as the mean gradients, an estimate of eddy diffusivity, K is determined and thus it is possible to parametrize the fluxes. For TKE $E = (\overline{(u'^2} + \overline{v'^2} + \overline{w'^2})/2$, the prognostic equation assuming horizontal surface homogeneity can be written as follows:

$$\frac{\partial E}{\partial t} = -\overline{u'w'}\frac{\partial U}{\partial z} - \overline{v'w'}\frac{\partial V}{\partial z} + \frac{g}{\theta}\overline{w'\theta'}$$
$$- \frac{\partial}{\partial z}\left(\overline{w'E} + \frac{\overline{pw'}}{\rho}\right) - \varepsilon, \tag{13}$$

where the first two terms on the RHS represents the contributions from shear, the third term represents the buoyancy forcing, the fourth turbulent transport and the fifth dissipation of turbulent energy. The vertical flux of temperature, $\overline{w'\theta'}$ flows down the local vertical gradient of temperature. In this, several terms in the RHS are parametrized (Stull, 1988). The last term ε (dissipation term) is also prognostically determined using

$$\frac{\partial \varepsilon}{\partial t} = a_1 \frac{\varepsilon}{E}\left[-\overline{u'w'}\frac{\overline{\partial U}}{\partial z} - v'w'\frac{\overline{\partial V}}{\partial z} + \frac{g}{\theta}\left(\overline{w'\theta'}\right)\right]$$
$$- a_2 \frac{\varepsilon}{E} + a_3\left(K_m \frac{\partial \varepsilon}{\partial z}\right), \tag{14}$$

where $a_1 = 1.44$, $a_2 = 1.92$ and $a_3 = 0.77$ (Basu et al., 1999) and $\overline{w'\theta'} = -K_h(\frac{\partial \overline{\theta}}{\partial z} - \gamma_{cg})$

The counter gradient term γ_{cg} is taken as 0.7×10^{-3} °K m^{-1}. The counter gradient term (which is against the local gradient) deals with the non-local effects. The eddy diffusivity is parametrized as $K = \frac{(0.3E)^2}{\varepsilon}$.

2.6. Unified model

An improved single model with the unified PBL scheme has been developed from the post processing of the superensemble, which is given in Appendix B. The notion of the unified model was originally developed for one of our earlier studies Krishnamurti and Sanjay (2003). The unified PBL scheme is built within a single model where the weighted sum of the PBL schemes is used. The method for the calculation of weights is identical to what we use for the construction of the superensemble. The unified PBL scheme increases the computing time of the model runs only minimally. This new PBL scheme is both statistical and physical based. It combines the physically based parametrization schemes based on their local past performances. This scheme is designed to correct the best parametrization scheme of the suite of models. Since this scheme is flexible in terms of the number of models in the ensemble, any number of input member models can, in principle, be used to construct the unified PBL scheme. This new

unified scheme is an integral part of one model and thus has the potential to improve forecasts of other parameters of the model in addition to the variable for which the scheme is built upon.

All the above PBL models share the same constant flux layer, that is the familiar surface similarity theory based on Businger et al. (1971). Our study makes a distinction between the stable and the unstable PBL, this is based on the Bulk Richardson number as seen by the surface similarity theory.

3. Data

Using a horizontal resolution of T170 (170 wave triangular truncation) and 27 vertical levels within the FSU global model, 110 2-d forecast runs were carried out using each of the five PBL schemes discussed in Section 2. Each set of five model runs carry the same initial states and all model physics and dynamics codes remain identical except for these different PBL formulations. Initial conditions to FSU GSM are obtained from the European Centre for Medium-Range Weather Forecasts (ECMWF) operational global analyses of zonal and meridional wind components, geopotential height, temperature and specific humidity. These analyses were produced using a four-dimensional variational data assimilation (4DVAR) scheme by the state-of-the-art ECMWF model with very fine spectral horizontal resolution (T$_L$319) and 50 σ-layers in vertical, and uses various types of conventional and non-conventional observations. These data sets were available to us on 0.5° × 0.5° grids over 15 standard pressure levels between 1000 and 10 hPa. These were interpolated to our model's horizontal spectral T170 resolution and 27 unequally spaced σ-layers in vertical. The next step is a Physical initialization (PI) that is described in the following section. The model topography was obtained from the United States Geological Survey (USGS) GTOPO30 data set—a global digital elevation model (DEM) on a regular latitude–longitude grid, whose horizontal grid spacing is 30 arc seconds. A resample version (5-min average) of this data set is interpolated to the model T170 spectral Gaussian grid. Detailed model description is provided in Appendix A and description of the superensemble methodology is provided in Appendix B.

4. Benchmark fluxes

Given a number of ways of computing the boundary layer fluxes, the validation of such schemes requires observed estimates of fluxes. That can come by from direct measurements of fluxes from field experiments. However those are limited to shorter periods and cover small regions where these field experiments are conducted. Models are constantly changing and to take current versions of boundary layer models and to validate against such regional past data sets did not seem very adequate. There is an indirect data product that provides somewhat useful global estimates for the PBL fluxes of moisture (or latent heat). This entails a two steps computational procedure: The first step is the

physical utilization (or rain rate utilization). The initialization carries three parts, restructuring the cumulus convection algorithm to yield nearly the same rainfall as provided by satellite estimates, a reverse similarity algorithm to arrive at PBL flux of moisture consistent with the observed estimates of rain, and a matching of model based Outgoing Long wave Radiation (OLR) to the satellite based estimates of OLR. A final step carries out a Newtonian relaxation of the modified moisture profile in a pre-forecast phase between hours –24 to hour 0. In our global model's physical initialization, we carry out all four steps to initialize the rain, Krishnamurti et al. (1991). The PBL flux estimates are obtained from a vertical integral of the Yanai et al. (1973) apparent moisture sink algorithm. That is described by the equation

$$\hat{Q}_2 = \int_{p_{\text{top}}}^{p_s} -L\left(\frac{\partial q}{\partial t} + \nabla \cdot \overline{qV} + \frac{\partial(\overline{q\omega})}{\partial p}\right). \qquad (15)$$

Knowing the precipitation estimates from the satellite and the values of $-L(\frac{\partial q}{\partial t} + \nabla \cdot \overline{qV} + \frac{\partial(\overline{q\omega})}{\partial p})$ from the physically initialized reanalysis it became possible to obtain the best estimates of the surface moisture (or latent heat flux) globally. This is how a bench mark estimate of 'observed' PBL flux estimates were obtained. Since the observed fluxes are not globally available, it is possible to exploit the following relations from Yanai et al. (1973) on the apparent heat source Q_1 and the apparent moisture sink Q_2 computed from

$$Q_1 = C_P \left(\frac{p}{p_0}\right)^\kappa \left(\frac{\partial \theta}{\partial t} + V \cdot \nabla \theta + \omega \frac{\partial \theta}{\partial p}\right)$$
$$= Q_R + L(c - e) - \frac{\partial \overline{s'\omega'}}{\partial p} \qquad (16)$$

$$Q_2 = -L\left(\frac{\partial q}{\partial t} + V \cdot \nabla q + \omega \frac{\partial q}{\partial p}\right) = L(c - e) + L\frac{\partial \overline{q'\omega'}}{\partial p}. \qquad (17)$$

Integrating RHS of (16) and (17) from the tropopause pressure P_T to the reference PBL pressure P_S, one can obtain a measure of the total upward heat flux at that level for each point of the globe. As explained before, an improved analysis of divergent winds and moisture in the tropics is obtained through physical initialization technique using Tropical Rainfall Measuring Mission (TRMM) derived rain rates. This is carried out using a Newtonian relaxation method during a pre integration phase where the fluxes, rainfall rates, and the cloud distributions provide a consistent humidity analysis and provide observed estimates of PBL fluxes for sensible heat and water vapour.

5. Discussion of results

In this section we present the results of latent heat fluxes at the $\sigma = 0.95$ level (which is roughly half kilometre above the earth's surface). The benchmark 'observed' flux estimates came from a combination of Yanai fluxes and the physically initialized rainfall estimate. The purpose of not selecting the surface layer for

model flux inter comparison is that all models shared surface similarity flux in the surface layer and are not based on the different PBL theories. We shall present here the performance skills of the member models, those for the ensemble mean, the unified model and the multimodel superensemble. We shall illustrate the results for the training phase and from the forecast phase of the multimodel performances. The evaluation of fluxes includes the domain average fluxes, the bias scores, the rms errors and the correlation of the model versus the observational estimates. Primarily the results for the monsoon domain are shown here, we also include some global estimates for the error statistics.

5.1. Geographical distribution of weights

For our forecasts out to 2 d we evaluate the geographical distributions of weights every 3 h during the training phase of the superensemble. The reasoning behind that being that some models, over certain regions, seem to perform better earlier in their forecasts and some perform better in the later hours. Thus weights are designed to vary in space and time. We will illustrate one such sample of weights for hour 3 of forecasts for the five different PBL schemes (Fig. 1a–e). Negative weights are shown by green and blue colours, reddish colours carry positive weights. The yellow colour shows smaller weights. It should be noted that the negative weights are statistical fit measures, they are the same as in any applications of statistical data that are subjected to multiple regression where the weights are determined via a least-square minimization principle. No hard physical interpretations should be expected for these negative weights. One should feel free to use such in meteorological problems. If the weights are positive for some models at some locations and are negative for other models at the same location it simply means that models with negative weights carry a negative correction with respect to the analysis fields. We have established in Chakraborty et al. (2006) that the weights of different models plotted against the forecast period, during the training phase, do very closely resemble the plots of correlations of model output versus the observed counterparts during the same training phase. Thus negative weights do seem to imply that those models have negative correlation against observations during the training phase. A robust spread of weight distributions are seen in four out of these five panels. Weights are uniformly closer to zero for the FOC scheme. This model evidently did not get weighed much in the construction of the unified model or the superensemble. A mix of positive and negative weights distributed over the tropics were needed to improve the forecasts of fluxes from the different schemes. The H&B carries locally large positive weights especially over Indochina, parts of the Pacific Ocean along 30°S, tropical eastern Pacific Ocean and the tropical Atlantic Ocean. These weights convey the complexity of the atmospheric boundary layer. No single scheme was found to uniformly describe the fluxes over the globe. Through these weights it is possible in principle to design a consensus model, we call it the unified model, which
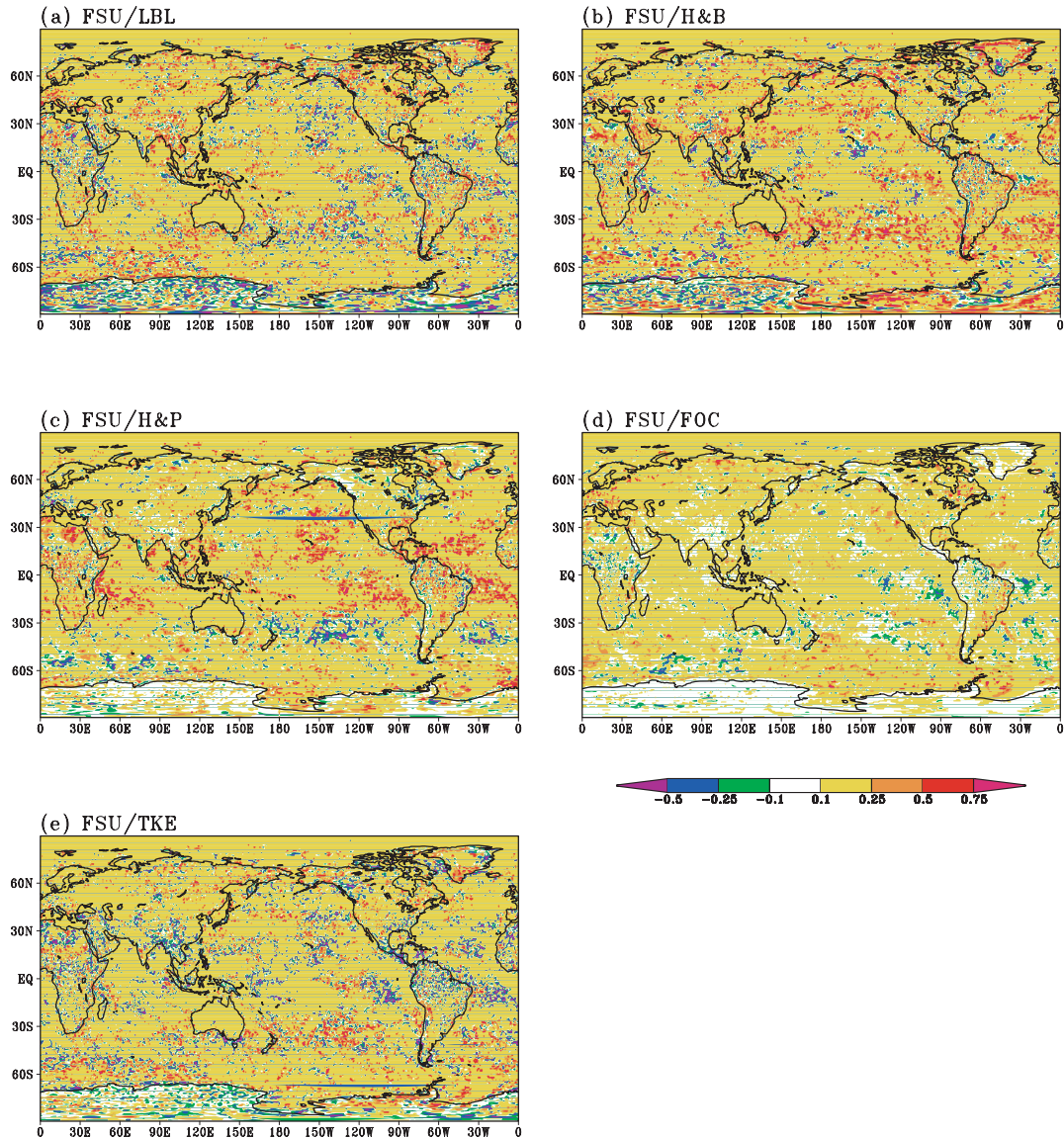
Fig. 1. Geographical distribution of superensemble weights for hour 3 of forecasts of PBL fluxes for different member models.

may perform better than individual models that carry a single scheme.

5.2. Assessment of models

The training period considered for the study is from 15 June 2002 to 22 September 2002 (100 d). The superensemble forecast phase is from 23 September 2002 to 30 September 2002. We have carried out a number of forecasts during the training and forecast phases using the member models, ensemble mean and the multimodel superensemble. We examined several case studies of monsoon disturbances in detail. Three of these were from the training phase of the superensemble. One case was examined from the forecast phase where the unified model was

also assessed. We shall provide a summary of results for all four cases however limit detailed discussions to one case each from the training and forecast phase of the superensemble.

5.2.1. A Well marked low pressure area during 20–28 June 2002. Under the influence of an upper air cyclonic circulation, a low pressure formed over the northwest Bay of Bengal off Orissa-Gangetic West Bengal coasts on 20 June. The associated cyclonic circulation extended up to mid tropospheric levels. It persisted on 21 June and became well marked over northeast Bay of Bengal off Bangladesh–Gangetic West Bengal coasts on 22 June. Following a west northwesterly track, it traversed up to southeast Rajasthan and adjoining northwest Madhya Pradesh (as a low pressure area) and dissipated on 29 June. Figure 2 shows the geographical distribution of fluxes for 21 June 2002.
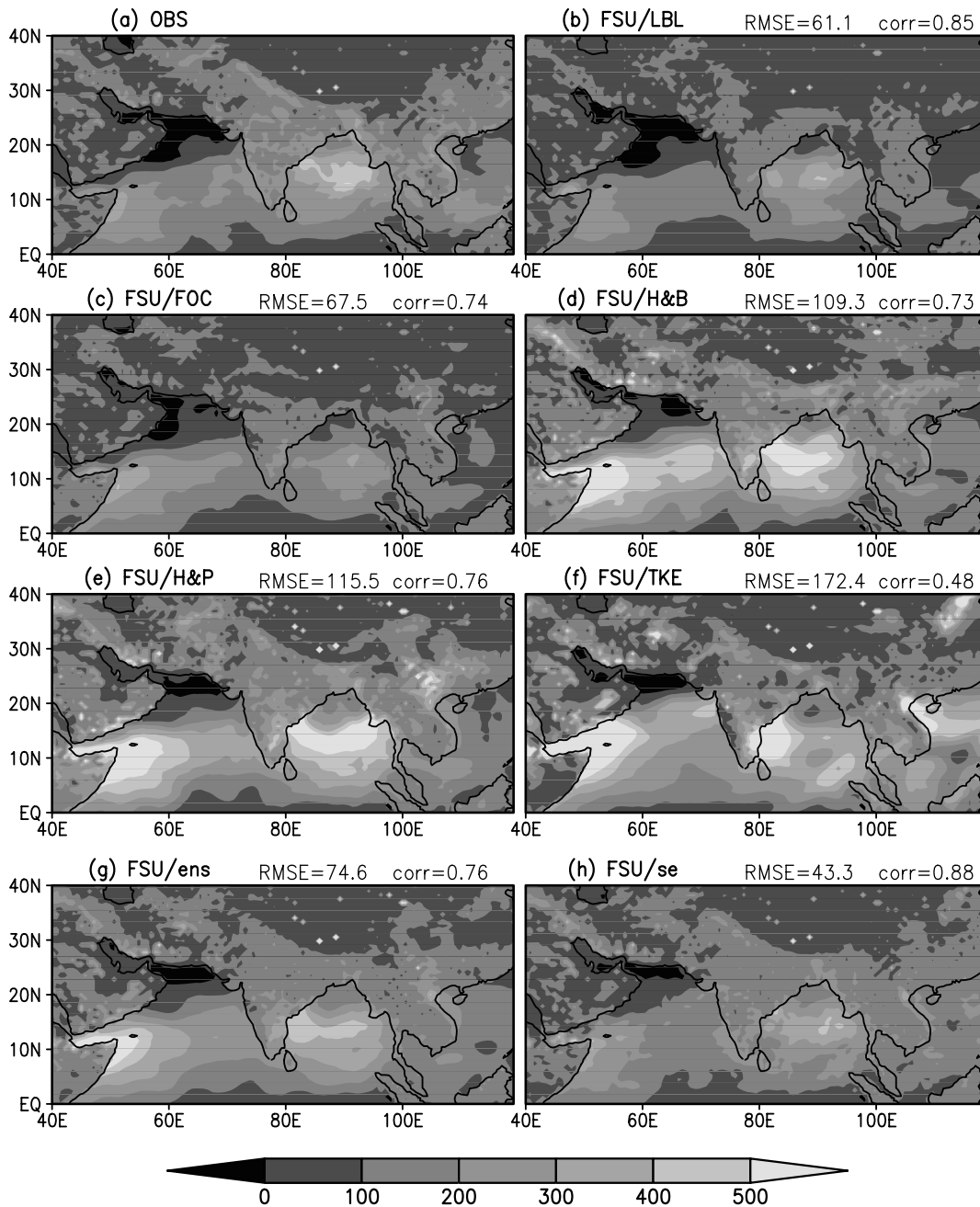
Fig. 2. Geographical distribution of Day 1 forecast of latent heat flux (Wm^{-2}) for 21 JUN 2002 over the monsoon domain (40°E–120°E, Eq-40°N).

From the figure, it is seen that H&B, H&P and TKE show rather large magnitudes of fluxes over the Bay of Bengal as well as the Arabian Sea that were not present in the observed estimates. In contrast, LBL, and FOC show a better distribution of fluxes especially over the Indian seas although they seem to underestimate them somewhat over the Bay of Bengal. The high magnitude of latent heat fluxes seen over the Arabian Sea and Bay of Bengal from the H&B, H&P and TKE gets reflected in the ensemble mean as well. The stronger fluxes seen in H&B, H&P and TKE

schemes arise from the stronger surface winds over the Arabian Sea and the Bay of Bengal. The fluxes downstream from Somalia over the Somali Jet region are in fact too strong compared to the benchmark fluxes. The H&B, and H&P schemes appear to overestimate the fluxes of moisture over regions of strong winds. The superensemble brings these fluxes closer to the benchmark estimates. It should however be noted that this case falls within the training phase, thus the superior results from the superensemble are no more than the goodness of fit of the superensemble
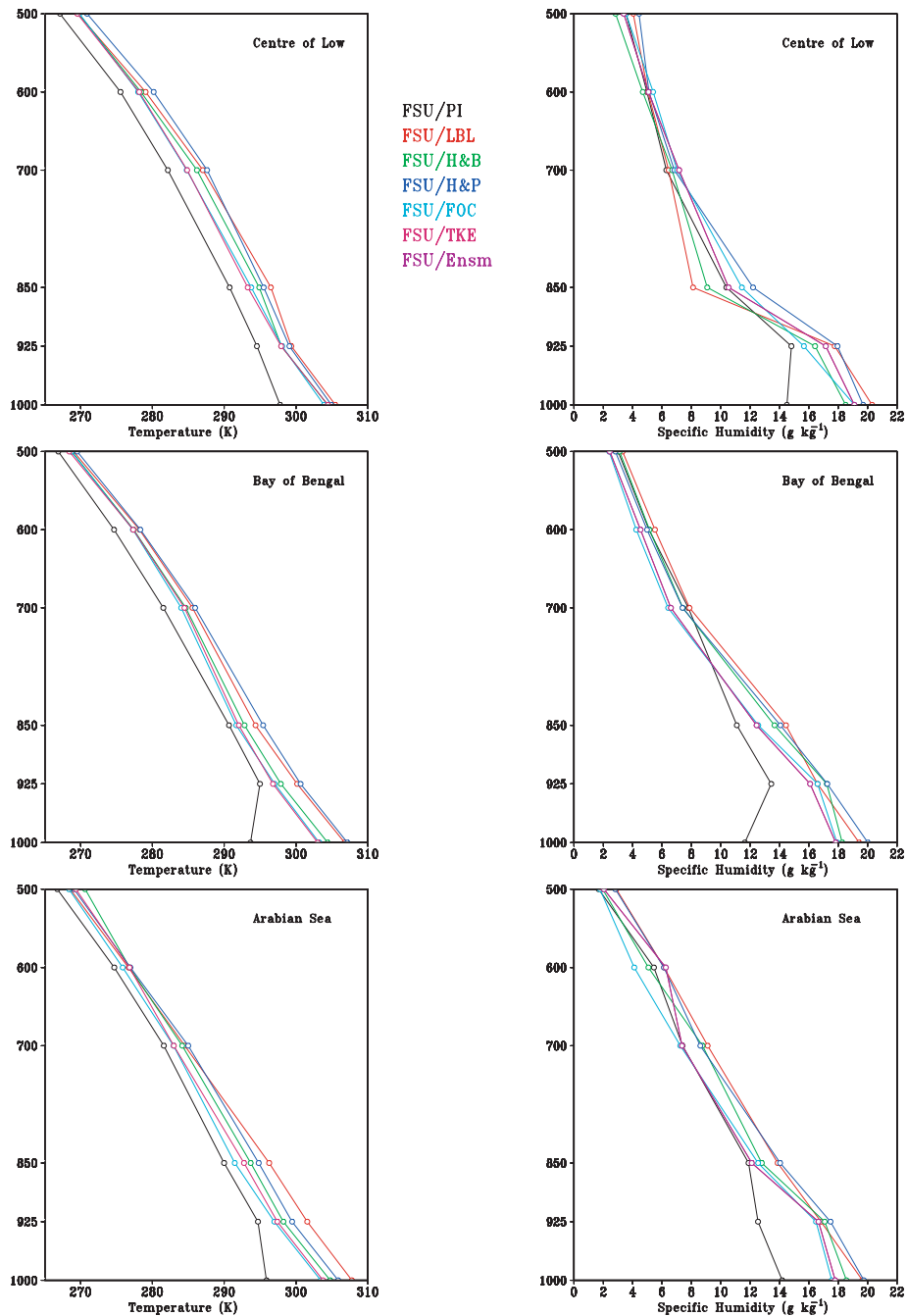
Fig. 3. Vertical profiles of temperature and specific humidity (valid at 12 UTC 21 June 2002) over three different regions viz. centre of the low (90°–91°E, 21°N), Bay of Bengal (90°–95°E, 10°–20°N) and Arabian Sea (70°–75°E, 10°–20°N).

procedure. These features of the fluxes also get reflected in the rainfall distributions by all the individual models, those are not illustrated here. The higher rainfall observed over the north central parts of India did not get reflected by any of the individual models. This was seen from the vertical profiles of temperature and specific humidity shown in Fig. 3, valid at 12 UTC 21 June 2002 (day 1 forecast) over three different regions viz. center of

the low (90°–91°E, 21°N), Bay of Bengal (90°–95°E, 10°–20°N) and Arabian Sea (70°–75°E, 10°–20°N).

5.2.2. Low pressure area during 15–18 August 2002. This was a second case that we had examined. Under the influence of an upper air cyclonic circulation, a low pressure had formed over coastal areas of north Orissa and adjoining northwest Bay of Bengal on 15 August. Subsequently, it moved in a west northwesterly
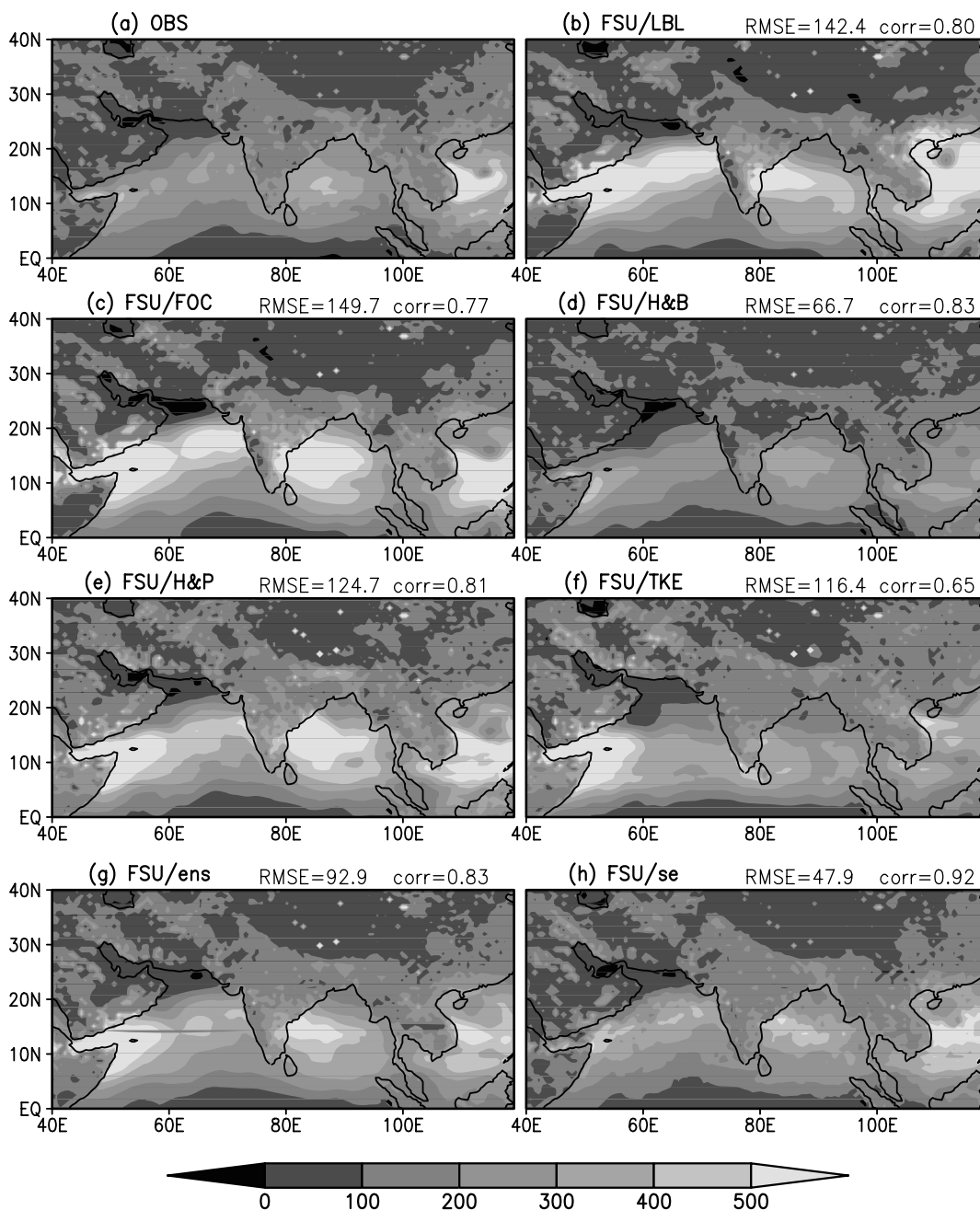
Fig. 4. Geographical distribution of Day 1 forecast of latent heat flux (Wm^{-2}) for 17 Aug 2002 over the monsoon domain (40°E–120°E, Eq-40°N).

direction up to north Madhya Pradesh and adjoining south Uttar Pradesh and became less marked on 19 August 2002. Figure 4 shows the geographical distribution of latent heat fluxes for 17 August 2002. From the figure it is seen that the LBL, H&P and the FOC schemes show the largest magnitudes of fluxes over the Bay of Bengal and Arabian Sea region, and like the previous case such large values were not seen in the observed estimates. In contrast, H&B and TKE show somewhat reasonable distributions of fluxes especially over the Bay of Bengal. However, none

of them are able to capture the magnitude as well as the distribution of the fluxes over the Asian landmass, except for the TKE model, which shows slightly better fluxes over the land region compared to LBL and H&B. The high magnitude of fluxes seen over Arabian Sea and Bay of Bengal by H&P, LBL and FOC also got reflected in the ensemble mean as well.

5.2.3. Low pressure area during 22–27 August 2002. This was the third case we studied in some detail. Under the influence of an upper air cyclonic circulation, a low pressure had formed
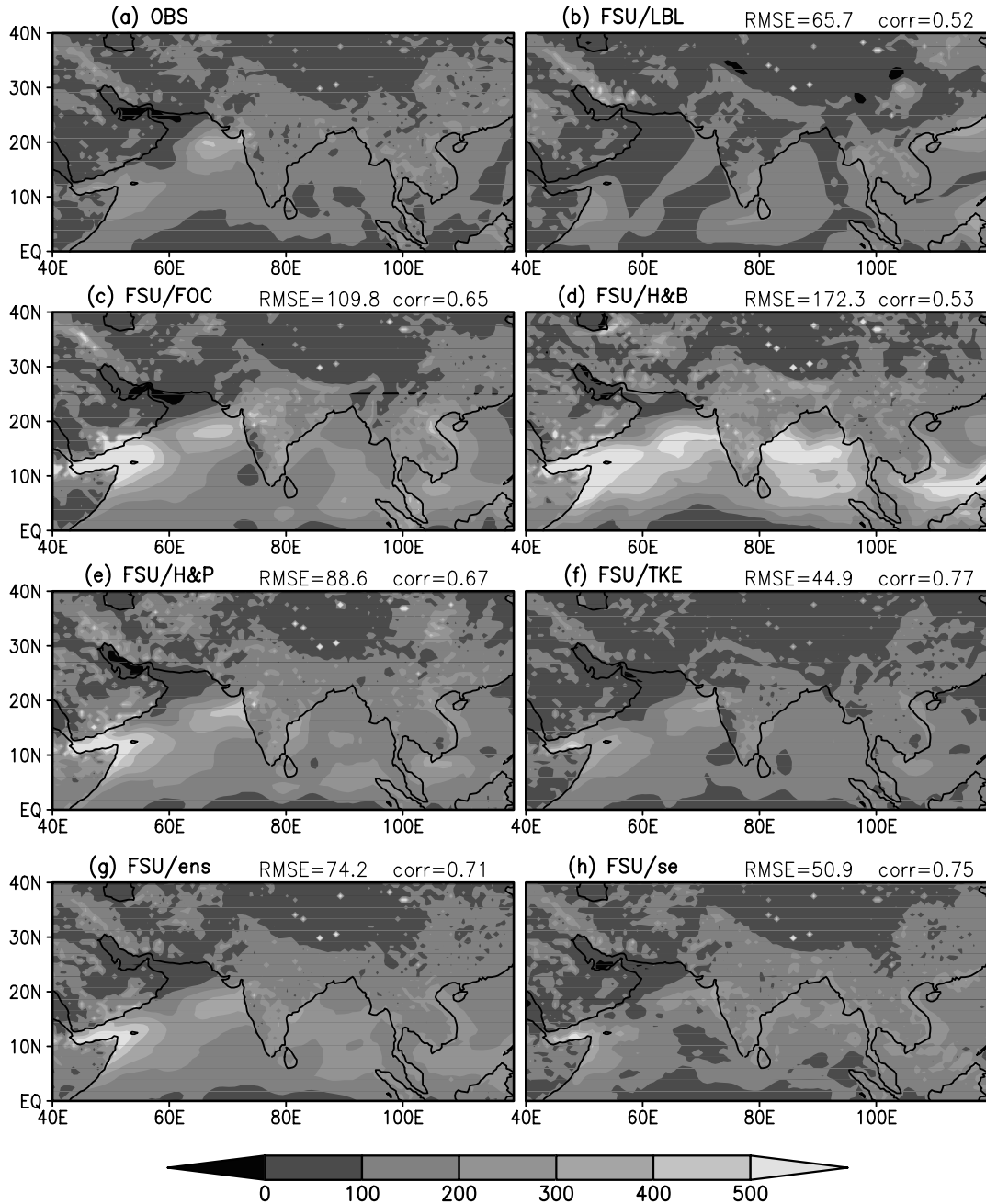
Fig. 5. Geographical distribution of Day 1 forecast of latent heat flux (Wm^{-2}) for 26 Aug 2002 over the monsoon domain (40°E–120°E, Eq-40°N).

over the northwest Bay of Bengal off coastal areas of Orissa and Gangetic West Bengal on 22 August 2002. Moving inland, this low was located over Orissa and adjoining areas of Chattisgarh and north Andhra Pradesh on 23 August, over Vidharbha and neighbourhood on 24 August, and over west Madhya Pradesh and adjoining areas of Maharashtra and Gujarat on 25 August. Subsequently it moved over Saurashtra and Kutch and neighbouring areas on 26 August and it finally moved over northeast Arabian Sea and neighbourhood on 27 August before becom-

ing less marked on 28 August. Figure 5 shows the geographical distribution of fluxes for 26 August 2002. Here we note that the models H&B and FOC carry larger magnitude of fluxes over the Arabian Sea, the fluxes of magnitudes 200–300 Wm^{-2} over Bay of Bengal were not seen in the observed estimates. In contrast, H&P and TKE show somewhat reasonable distribution of fluxes especially over these Indian seas. These three models contributed reasonable fluxes over the Asian subcontinent. The LBL model tends to underestimate the fluxes over most of the land areas.

The high magnitude of fluxes seen over Arabian Sea and Bay of Bengal by H&B and FOC also got reflected in the ensemble mean. These schemes showed a larger dependence of fluxes to wind intensities.

5.2.4. A well marked low pressure area during 19–26 September 2002. This case was the fourth case we studied which falls during the forecast phase. During this late monsoon period, under the influence of an upper air cyclonic circulation, a low pressure area formed over east central and adjoining northeast Bay of Bengal on 19 September. It moved over to northern parts of central Bay and adjoining northern Bay and became well marked over there during late 20 September. It persisted over the oceanic area till the 24 September. Moving inland, it became a low pressure over Bihar and neighboring areas of Jharkhand and Gangetic west Bengal on 25 September and subsequently became less marked by the 26 September evening. Figure 6 shows
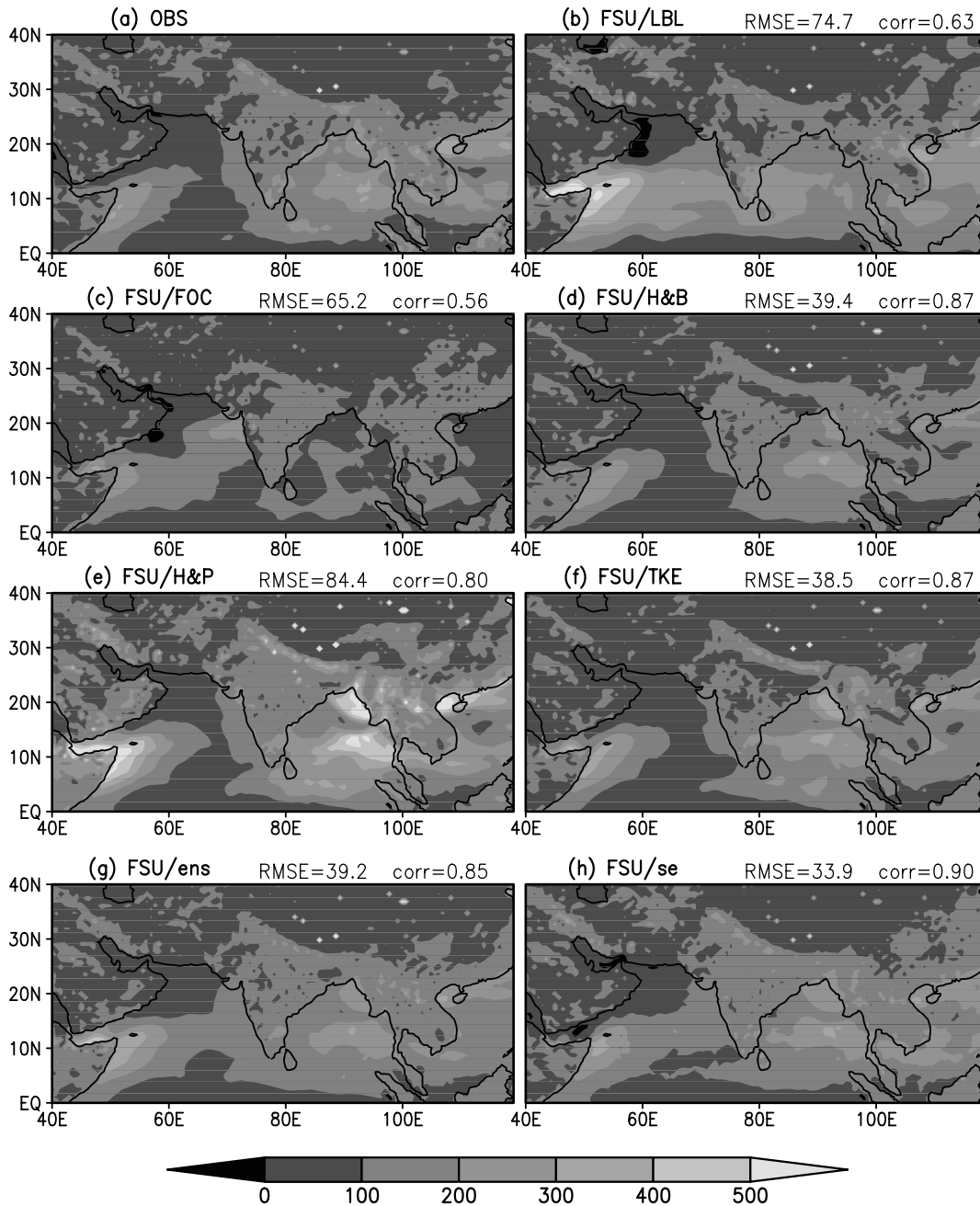
Fig. 6. Geographical distribution of Day 1 forecast of latent heat flux (Wm^{-2}) for 20 Sep 2002 over the monsoon domain (40°E–120°E, Eq-40°N)

Table 1. Domain averaged latent heat fluxes and skill scores during the case studies (monsoon domain)

Models	Case: (a) 20–28 Jun 02 Well marked low (Mean flux = 136)			Case: (b) 15–18 Aug 02 Low pressure (Mean flux = 158)			Case: (c) 22–27 Aug 02 Low pressure (Mean flux = 123)			Case: (d) 19–26 Sep 02 Well marked low (Mean flux = 118)		
	Mean	rms	cc	Mean	rms	cc	Mean	rms	cc	Mean	rms	cc
LBL	97	51	0.91	145	68	0.77	139	58	0.74	151	82	0.63
FOC	223	146	0.80	197	98	0.76	147	62	0.80	134	46	0.82
H&B	169	86	0.76	132	61	0.84	195	117	0.74	98	35	0.91
H&P	188	91	0.84	229	121	0.81	164	79	0.78	156	69	0.82
TKE	176	74	0.84	126	73	0.78	116	35	0.87	110	29	0.91
Ens	171	70	0.86	166	63	0.82	152	62	0.81	129	37	0.87
Sens	139	25	0.94	148	41	0.93	136	37	0.87	127	28	0.92

the geographical distribution of fluxes for 20 September 2002. From the figure it is seen that almost all the models showed flux distributions over the Bay of Bengal although the H&P model showed an over prediction. There was practically no appropriate flux distribution shown over the Arabian Sea by most of the models except over the horn of Africa. Here again H&P showed some over-prediction by about 100 Wm^{-2}. The ensemble mean showed a reasonably good prediction of fluxes and is in good agreement with the observed estimates.

In Table 1, we present a summary of the domain averaged latent heat fluxes and skill scores for the aforementioned case studies. Here we have included separate summaries for all the four case studies. The top boxes include the observed estimates of the mean latent heat fluxes in Wm^{-2}. The rows include the case study averaged model fluxes. This table suggests some overall consistencies in the performance of the models. The LBL is the simplest local closure scheme that seems to underestimate the fluxes for the June and the mid August cases. For the late August case it slightly overestimated the fluxes, and for the late September case the LBL carried stronger than the observed fluxes of latent heat. The FOC is one of the two local closure schemes, and this one contains parameters that make the latent heat fluxes generally larger than those of LBL. That was noted for the mean fluxes of June and August cases. For the late monsoon season case the mean latent heat fluxes for the LBL and FOC were large compared to the observed estimates. Overall the non-local schemes H&B and H&P contributed to larger fluxes. The TKE and the ensemble mean were somewhat comparable, that is, those fluxes were close to the average of the member model fluxes. Clearly the latent heat fluxes from the superensemble were closest to the observed estimates in a consistent manner. Generally that hierarchy of performance was also clearly reflected in the rms errors and the correlation of the member model fluxes to the observed estimates. For the late monsoon case, in September we noted same anomalous behaviour from the LBL (too large fluxes)

and H&B (too small fluxes). That seemed to be related to very low values of Richardson number in the PBL during September. The multimodel superensemble carried consistently high skills for all cases, that is, in general lowest rms errors and the highest correlation.

We have also performed these same calculations for different months covering each day of computation (Table 2). These are also shown for the same monsoon domain. These cover periods: June 15 to June 30, July 1 to 31, August 1 to September 22, and the superensemble forecast period September 23 to 30, all for the year 2002. Here again we note some uniformity in the member model's performance from one month to the next, but we also note some minor differences. In general the superensemble carries the best forecasts in terms of monthly mean latent heat fluxes showing the lowest rms errors and the highest correlation with respect to the observed estimates. The local closure scheme FOC and the non-local closure scheme H&P systematically overestimate the latent heat fluxes and the local scheme LBL (in general) underestimate the fluxes. The TKE scheme overestimates the fluxes in the warm month of June, and thereafter the TKE fluxes gradually seem to go towards the low side. This suggests that the TKE carries larger fluxes in the drier part of the monsoon season and starts to underestimate the fluxes as the wet monsoon season advances. It is interesting to note that the rms error of superensemble is in the range of 10–30 Wm^{-2} and carries a correlation in excess of 0.9 for all months. The ranges of monthly averaged rms errors for the member models are even as large as 146 Wm^{-2} and the lowest correlation were around 0.63. The superensemble carried the highest skills, that is no more than a goodness of fit of the statistics since June, July, August and part of September were in the training phase. The skills of the LBL during August and September began to get much lower and the TKE was clearly the best model in the forecast phase during September. The correlations of the superensemble forecasts over the global tropical belt (30°S to 30°N) and the monsoon belt were 0.94 and 0.90, respectively. This shows that pattern

Table 2. Domain averaged latent heat fluxes and skill scores for training and forecast phases (monsoon domain)

Models	(a) 15–30 Jun 02 (Observed Mean flux = 134) (Training phase)			(b) 01–31 Jul 02 (Observed Mean flux = 142) (Training phase)			(c) 01 Aug - 22 Sep 02 (Observed Mean flux = 131) (Training phase)			(d) 23–30 Sep 02 (Observed Mean flux = 108) (Forecast phase)		
	Mean	rms	cc	Mean	rms	cc	Mean	rms	cc	Mean	rms	cc
LBL	96	50	0.91	99	55	0.91	147	53	0.83	134	69	0.63
FOC	220	140	0.80	201	103	0.87	161	70	0.82	144	65	0.78
H&B	175	87	0.79	134	30	0.93	135	35	0.90	89	33	0.90
H&P	184	89	0.83	188	79	0.88	180	83	0.83	135	54	0.79
TKE	165	67	0.83	129	30	0.93	118	31	0.91	100	28	0.90
Ens	168	68	0.86	150	37	0.92	148	49	0.87	120	37	0.84
Sens	137	24	0.95	131	19	0.98	136	12	0.99	120	30	0.90

correlation for latent heat fluxes can be improved in the superensemble forecasts.

5.3. Overall model skills over the globe and the monsoon domain

During the forecast phase, the results of latent heat fluxes at the $\sigma = 0.95$ level, from a two day forecast, over the monsoon do-

main (start date 15Z23SEP2002) are shown in Fig. 7a–d. These carry, respectively the mean values, the bias, the root mean square errors and the correlation coefficients of the model fluxes against the observed estimates of latent heat fluxes (all of these pertain to the monsoon domain, equator to 40°N and 40°E to 120°E). During the forecast period, the mean fluxes from the member models show spread of fluxes ranging from roughly 50 to 280 Wm^{-2}. The observed fluxes (open circles) and those based
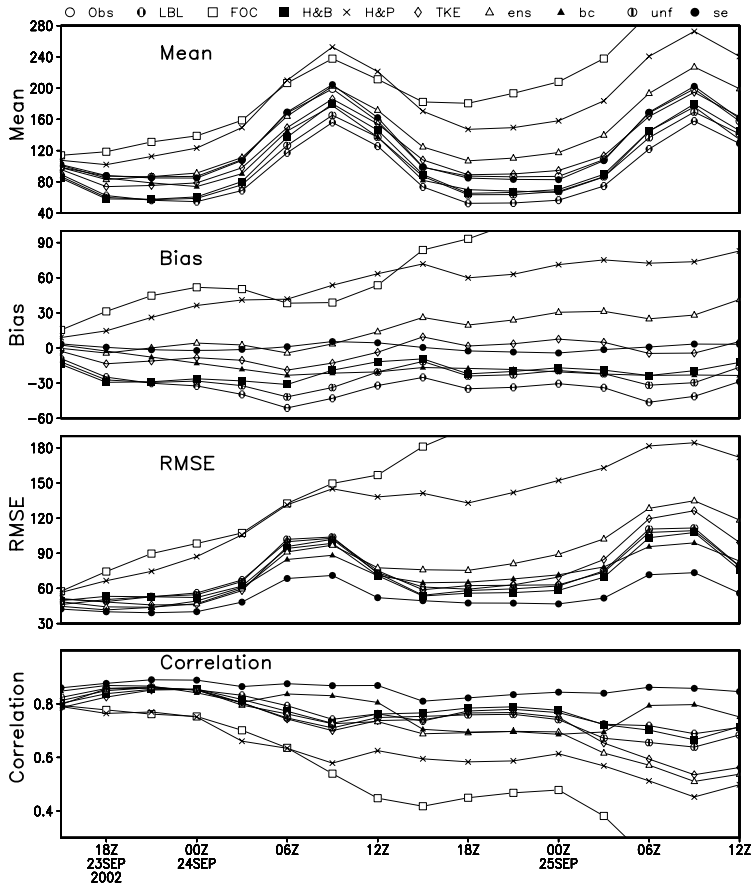

Fig. 7. Skill scores of 2 d surface latent heat flux forecasts with IC at 12 UTC 23 Sep 2002 over the monsoon domain.

on the superensemble (closed circle) follow each other very closely. This shows that it is possible to forecast the moisture fluxes reasonably by the superensemble. These results certainly depend on the observed measures that were used to train the dependent variables of the model forecasts. If another benchmark observed forecasts were available, from our past experience, we can state that the superensemble would still outperform all member models forecasts. A bias score of zero is considered the best forecast. The spread of the bias for the member models (for latent heat fluxes) show a spread between roughly -45 and 200 Wm^{-2}. The superensemble biases stay very close to zero (± 5 Wm^{-2}) throughout the forecast. Both the rms errors and the correlation coefficients of the model latent heat fluxes versus the observed estimates show a consistent superior forecast for the PBL fluxes from the superensemble. The average rms error of the fluxes, during the two days is the least for the superensemble and is around 25 Wm^{-2} whereas the spread from models rms errors range from 60 to 220 Wm^{-2}. The correlations are consistently the highest for the superensemble and stay around 0.9 throughout the forecasts. The correlation of the member models shows a spread (roughly) of 0.4–0.8.

An averaged display of latent heat fluxes for the monsoon and the global domains for day 1 of forecasts (covering the period 1200 UTC 24 September to 1200 UTC 25 September 2002) are shown in Fig. 8a and b. Here we show (as vertical bars) the model and the observation-based estimates of latent heat fluxes in Wm^{-2}). In sequence from left to right are the observed heat fluxes, fluxes from the models (LBL, FOC, H&B, H&P and TKE, respectively), the ensemble mean, the unified model and the multimodel superensemble. The superensemble carries the best forecasts for the fluxes and stand out for both the monsoon and the global domain. These show the best agreement to the observed flux estimates (close to 120 Wm^{-2}). The FOC and the H&P schemes overestimate the latent heat fluxes, and the remaining three models underestimate them. Among the models, the mean latent heat fluxes are better handled by TKE compared to the other member models. The ensemble mean provides a somewhat better representation of fluxes compared to TKE. The behaviour of the unified model seems to vary somewhat from case to case, it seemed to perform better in strong rainfall cases and not as well over the undisturbed region where the member model variability was larger.

The geographical distributions of the latent heat flux (in the PBL at the $\sigma = 0.95$ level) illustrated in Fig. 9 are the 24 h forecasts valid at 1200 UTC 24 September 2002. The rms errors and correlation coefficients over the monsoon domain for the same period are illustrated on the panels. Panel (a) carries the observed estimates, panels (b–f) carry the member model fluxes, the
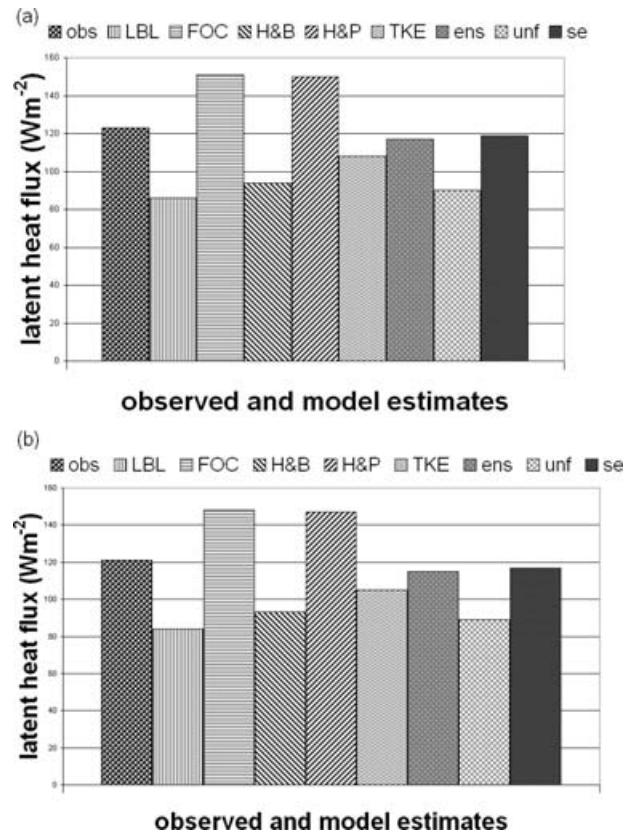

Fig. 8. Average latent heat flux in Wm^{-2} during the period 15 UTC 24 SEP to 12 UTC 25 Sep, 2002 (a) over the monsoon domain (b) over the globe.
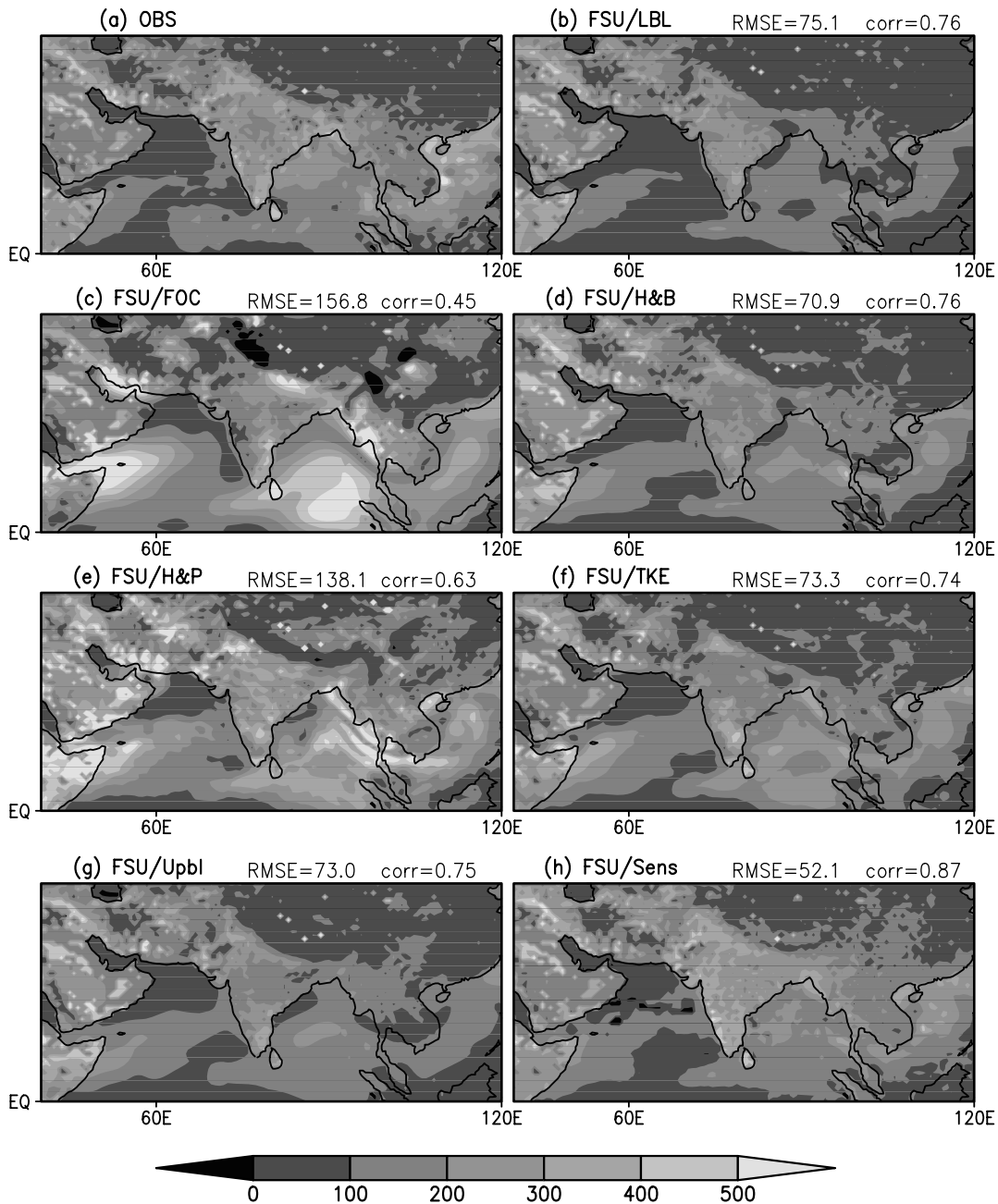
Fig. 9. Geographical distribution of 24-h forecasts of latent heat flux valid at 12 UTC 24 Sep 2002 over the monsoon domain.

results from the unified model are shown in panel g and those from the superensemble are in panel (h). It is clear that the multimodel superensemble describes the best geographical distributions. We also see that the models H&B and H&P (especially) carry the largest fluxes of latent heat. Those are overestimates over the oceans. The TKE method (panel f) appears to underestimate the fluxes and, the unified model appears to carry somewhat lower values as compared to the observed measures. The correlation and the rms error show that the superensemble carries

the best scores and the TKE is a close second and is the best among the individual member models. The results shown here are consistent with the averaged fluxes presented in the previous sections.

The performance of the unified model is shown in Figs. 10 and 11. The eight panels of both the figures carry the observed estimates and the forecast fluxes of latent heat from five member models, the unified model and the superensemble. Figures 10 and 11 carry the hour 3 and hour 48 of these fluxes. The RMS
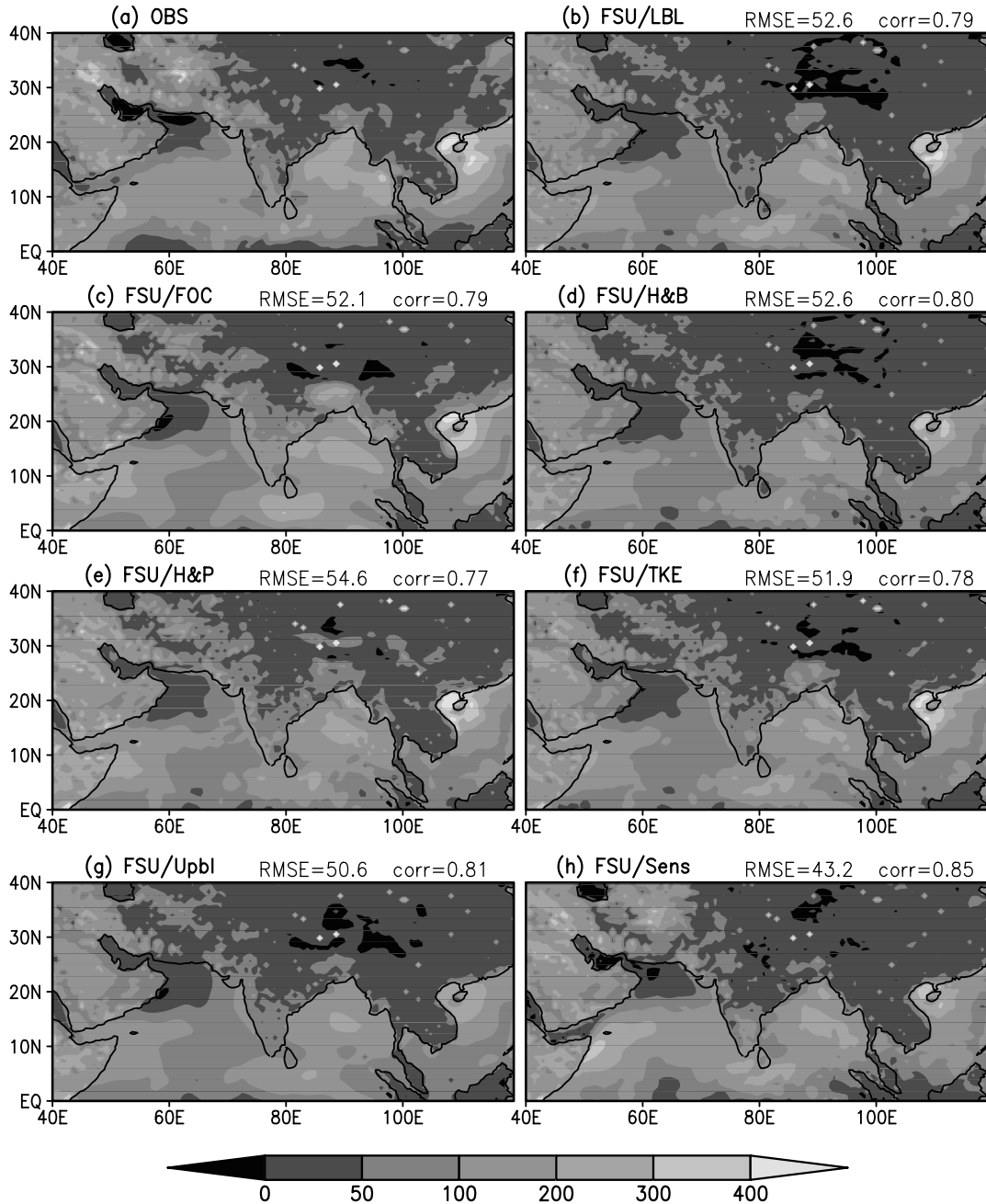
Fig. 10. Geographical distribution of 3-h forecasts of latent heat flux valid at 15 UTC 25 Sep 2002.

errors and the correlation (between respective model fluxes and observed estimates) are shown at the top of each panel. This shows that the unified model carries higher skills for 3 h of forecast compared to member models. The superensemble stands out the best. The unified model is still very impressive at hour 48, its performance is close to the best model (H&B). As the forecast proceeds in time the local closure model FOC and the non-local closure model H&P overestimate the fluxes drastically and carry the lowest skill scores. The skills of the superensemble remain

almost the same from hour 3 to hour 48 forecasts. However, the skill deteriorates in the member models as the forecast time increases.

6. Summary and concluding remarks

This is the third in a sequel of three papers (see also Krishnamurti and Sanjay, 2003; Chakraborty et al., 2006) where several different physical parametrizations were
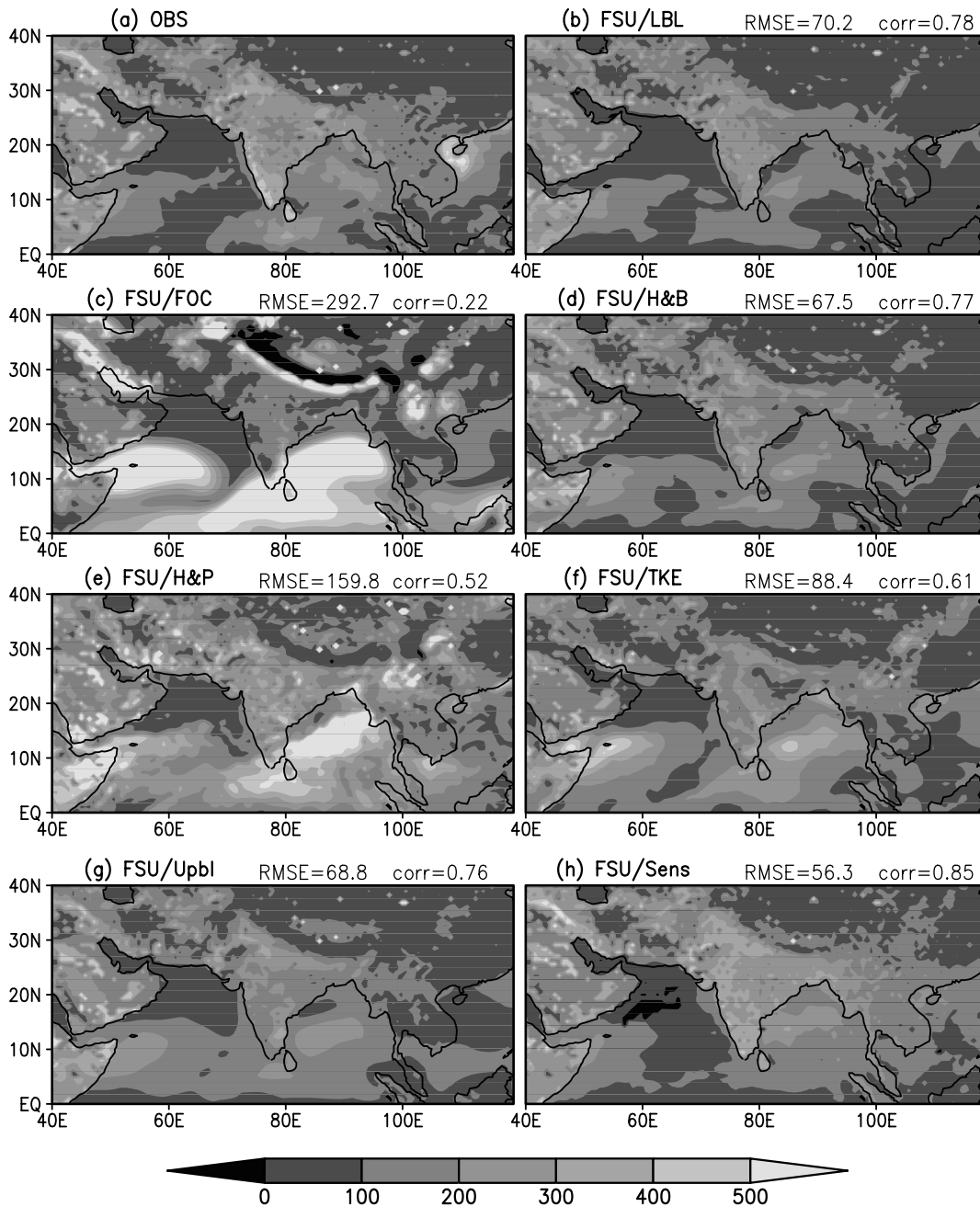
Fig. 11. Geographical distribution of 48-h forecasts of latent heat flux valid at 12 UTC 27 Sep 2002.

examined within a single model. Nearly 100 NWP experiments, using a sequence of initial states, preserving the rest of the model dynamics and physics, were carried out with each model. In all of the experiments we covered the period 15 June to 30 September 2002. Each day a forecast experiment was carried out using a different PBL scheme within the FSU global spectral model. All of these experiments utilized the same resolution, dynamics and rest of physics. All the initial states for a set of five forecasts were identical. We first examined the performance skills of a

single model by deploying a single physical parametrization at a time. Those experiments showed considerable differences in model skills.

Addressing cumulus convection algorithm, Krishnamurti and Sanjay (2003) deployed six different cumulus parametrization schemes that included the FSU modified Kuo Scheme, GSFC Relaxed Arakawa-Schubert Scheme, NRL-NOGAPS Relaxed Arakawa-Schubert Scheme, NCEP simplified Arakawa Schubert Scheme, NCAR Zhang-McFarlane Scheme, and NRL-NOGAPS
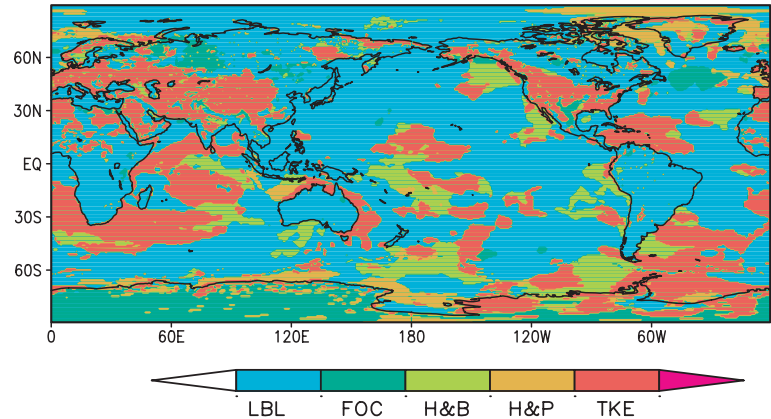
Fig. 12. Geographical distribution of models with least bias scores: 1-LBL(blue), 2-FOC(dark green), 3-H&B(light green), 4-H&P(light brown) and 5-TKE(red).

Emanuel Scheme. Krishnamurti et al. (2007) and Chakraborty et al. (2006) deployed four different cloud radiative transfer schemes that included an emissivity absorbtivity scheme and a band model for short- and long-wave irradiances parametrization schemes, NCAR CCM3 and Pleim-Xiu cloud parametrization schemes. This present study brings in five different PBL schemes. We have examined the performance of the FSU global spectral model for NWP forecasts using these different schemes. We noted that large systematic errors result from the deployment of these individual schemes for precipitation, fractional clouds and moisture fluxes within the PBL. It became clear from these exercises that uncertainties in physical parametrization schemes are as important as the initial data uncertainties. This brings up the issue of ensemble forecasts for the reduction of such uncertainties. In that context we have evaluated the ensemble mean and the FSU superensemble forecasts for all these three sets of physical parametrization experiments. The superensemble methodology carries a geographical spread of weights during the training phase, that is, the hind cast phase. The weights are generated using a multiple regression of forecast fields against the observed (analysis) counterparts. Krishnamurti and Sanjay (2003) used the observed precipitation estimates against the model's total rain for the derivation of the statistical weights in models that used diverse cumulus parametrization schemes.

In the present study the diverse PBL schemes provided fluxes of moisture in the PBL. Those were regressed against an observed counterpart derived from a mix of the Yanai's apparent moisture sink and physically initialized observed rainfall estimates. In order to have some measure of ground truth we made use of the vertically integrated equation for the apparent moisture sink. That was calculated at each grid point of the global model using reanalysis data sets that had been subjected to a rain rate initialization. The residual of this exercise was the PBL flux of moisture. This is regarded as a reliable 'observed' measure of PBL fluxes. We noted that in general the schemes FOC and H&P overestimated the fluxes whereas the schemes LBL and TKE carried weaker fluxes. We noted a stronger dependence of PBL fluxes to the surface wind speed for the LBL scheme,

it seemed to carry strongest fluxes over the strong wind region downstream from Somalia and over the central Bay of Bengal. Overall it was apparent that all of these schemes carried large systematic errors.

Figure 12 is a summary diagram on the geographical distribution of the member models that carries the best bias score. Here these summaries cover the entire period between June 15 and September 30, 2002. Here we use a colouring scheme: LBL (blue), FOC (dark green), H&B (light green), H&P (light brown) and TKE (red). It is clear that none of the PBL algorithms perform the best over the entire region. Here the TKE scheme performs the best over Indian Ocean, the southern latitude oceans, most of North America, Caribbean and in the belt of 30°N to 50°N over Asia and Europe. The preponderance of blue colour over South America, South Africa, and the Atlantic and Pacific oceans shows the higher skills of the local closure scheme LBL. There are few regions with light green where the skill of the H&B scheme is the highest. We deliberately did not include the bias scores of the superensemble in Fig. 12 as it outweighs all other models globally.

The aim of most model developers is to improve a single model towards a better performance from the changes that are made in the model. In that context we asked the question if a single model could be improved by bringing in a weighted sum of all of the above schemes. These weights are simply extracted from the aforementioned training phase of the superensemble where 'observed' counterparts are regressed against model forecast fields for convection, clouds and PBL fluxes respectively. All of the physical parametrization schemes are physically based hence their weighted sum likewise is also physically based. These weights vary in the three-dimensional space based on their past performance. We tagged such models as a single 'Unified model'. These three single models were run separately for cumulus parametrization (Krishnamurti and Sanjay, 2003), for cloud radiative transfer (Chakraborty et al., 2006) and for the PBL fluxes (the present paper). We noted that in all of the forecast experiments, the unified scheme within a single model performed better than all or most of the individual models that utilized a

single physical parametrization scheme. However we also found that the multimodel superensemble provided results that carried less error compared to the unified scheme as well. The implication of these results may be far reaching. It is very difficult to hope for an improved single model that utilizes a single physical parametrization scheme. Even if we were to develop such a single parametrization scheme within a single model, most likely a single model with a unified physical parametrization scheme would outperform that. In addition, a multimodel superensemble based on a family of single models with single physical parametrization scheme 'within each model' would outperform the unified model. All of this stems from the uncertainties in physical parametrization that show a behaviour quite analogous to those of initial data uncertainties. There is clearly a need for reliable observational estimates of latent heat fluxes both to support the model estimates and understand the physics.

7. Acknowledgments

8. Appendix A: An outline of FSU global spectral model

The global model used in this study is identical in all respects to that used in Krishnamurti et al. (1991). The T170 version of the model, however, has been highly vectorized to reduce the model integration time. An outline of the model is as follows:

1. *Independent variables:* $\lambda, \theta, \sigma, t$
2. *Dependent variables:* vorticity, divergence, temperature and specific humidity.
3. *Horizontal resolution:* Triangular spectral truncation; T170 resolution has a 512×256 Gaussian transform grid with a horizontal separation of about 80 km at $20°$ latitude.
4. *Vertical resolution:* There are 27 layers in the vertical between 50 mb and 1000 mb. Model variables are staggered in the vertical using Charney–Phillips vertical discretization.
5. *Time integration scheme:* The divergence equation, thermodynamic equation and pressure tendency equation are integrated implicitly while explicit time integration scheme is used for vorticity equation and moisture continuity equation. The tendencies of the physical processes are integrated using a forward time integration scheme.
6. *Space differencing scheme:* Spectral in the horizontal; centred differences in the vertical for all variables except moisture which is handled by an upstream differencing scheme.
7. Surface topography is based on envelope orography (Wallace et al., 1983).

8. *Parametrization of physical processes:* (a) Deep convection: based on the NCEP Simplified Arakawa-Schubert cumulus parametrization scheme (Pan and Wu, 1995), with a saturated downdraft. Cloud ensemble is reduced to only cloud type with detrainment only from its top. It includes the effects of moisture detrainment from convective clouds, warming from environmental subsidence, and convective stabilization in balance with the large-scale destabilization rate; (b) Shallow convection (Tiedke, 1984); (c) Dry convection; (d) Large-scale condensation (Kanamitsu, 1975). The scheme accounts for evaporation of falling precipitation; (e) PBL fluxes of heat, moisture and momentum are calculated using similarity theory (Businger et al., 1971); (f) Vertical distribution of fluxes in the free atmosphere is based on stability (Richardson number) dependent exchange coefficient (Louis, 1979); (g) fourth order horizontal diffusion (Kanamitsu et al., 1983); (h) Long- and short-wave radiative fluxes are based on band model and incorporate the radiative effects of water vapour, carbon dioxide, ozone and clouds (Lacis and Hansen, 1974; Harshvardan and Corsetti, 1984); (i) Parametrization of low, medium and high clouds for radiative transfer calculation is based on threshold relative humidity; (j) Surface temperatures: Prescribed over the oceans, whereas over the land, a surface energy balance coupled to the similarity theory determines the surface temperature including its diurnal cycle (Krishnamurti et al., 1991).

9. *Non-linear normal mode initialization:* (Kitade, 1983).
10. *Other boundary conditions*: Snow: monthly ($1° \times 1°$); SST: NCEP's $1° \times 1°$ weekly data Terrain: US Navy 5 min data; Vegetation US Navy 5 min data.

9. Appendix B: A description on superensemble methodology

The superensemble approach is a recent contribution to the general area of weather and climate forecasting, developed at FSU; this has been discussed in a series of publications, Krishnamurti et al. (1999, 2000a, b, 2001). This technique entails the partition of a time line into two parts. One part is a 'training' phase, where forecasts by a set of member models are compared to the observed or the analysis fields with the objective of developing a statistics on the least-squares fit of the forecasts to the observations and the second part is the forecast phase where estimates for a_i from the training phase are used to create the superensemble prediction. The performance of the individual models is obtained in the training phase using multiple linear regression against observed (analysis) fields. The outcome of this regression is the weights assigned to the individual models in the ensemble, which are then passed on to the forecast phase to construct the superensemble forecasts. In fact the temporal anomalies (model) of the variables are regressed against the observed anomalies and so in formulating the superensemble forecasts, the weights are multiplied to the corresponding model anomalies. The constructed forecast is $S = \overline{O} + \sum_{i=1}^{N} a_i(F_i - \overline{F_i})$.

Where $\overline{O}$ is the observed climatology over the training period; a_i is the weight for the ith member in the ensemble; and F_i and $\overline{F_i}$ are the ith model's forecasts and the forecast mean (over the training period) respectively. N is the number of member models. The weights a_i are obtained by minimizing the error term G, where $G = \sum_{t=1}^{N_{\text{train}}} (S_t' - O_t')^2$.

Here N_{train} is the number of time samples in the training phase, and S_t' and O_t' are the respective superensemble and observed field anomalies at training time t. This exercise is performed at every model grid points. The skill of the multimodel superensemble method significantly depends on the error covariance matrix (built with the model field anomalies F_i' and F_j', where F_i' and F_j' are the ith and jth model anomalies, respectively), since the weights of each model are computed from the designed covariance matrix $C = [c_{i,j}] = [\sum_{t=1}^{N_{\text{train}}} F_i'(t) F_j'(t)]$.

The construction of the superensemble utilizes a least-square minimization principle within a multiple regression of model output against observed (analysis) estimates.

References

Businger, J. A., Wyngaard, J. C., Izumi, Y. and Bradley, E. F. 1971. Flux profile relationship in the atmospheric surface layer. *J. Atmos. Sci.* **28**, 181–189.

Basu, S., Iyengar, G. R. and Mitra, A. K. 2002. Impact of a Nonlocal Closure Scheme in a simulation of a monsoon system over India. *Mon. Wea. Rev.* **130**, 161–170.

Basu, S., Raman, S., Mohanty, U. C. and Rajagopal, E. N. 1999. Influence of planetary boundary layer physics on medium-range prediction of monsoon over India. *Pure Appl. Geophys.* **155**, 33–55.

Blackadar, A. K. 1979. High resolution models of the planetary boundary layer. Advances in Environmental and Scientific Engineering I. Gordon and Breach.

Chakraborty, A., Krishnamurti, T. N. and Gnanaseelan, C. 2006. Prediction of the diurnal change using a multimodel superensemble. Part II: clouds, *FSU Report 2006, 2006–07*, 56 pp.

Deardorff, J. W., 1972. Theoretical expression for the counter-gradient vertical heat flux. *J. Geophys. Res.* **77**, 5900–5904.

Harshvardan and Corsetti, T. G. 1984. Long wave parameterization for the UCLA/GLAS GCM. NASA Tech. Memo. 86072, Goddard Space Flight Center, Greenbelt, MD, 52 pp.

Holtslag, A. A. M. and Boville, B. A. 1993. Local versus nonlocal boundary layer diffusion in a global climate model. *J. Climate* **6**, 1825–1847.

Holtslag, A. A. M. and Moeng, C.-H. 1991. Eddy diffusivity and countergradient transport in the convective atmospheric boundary layer. *J. Atmos. Sci* **48**, 1690–1698.

Hong, S.-Y. and Pan, H.-L. 1996. Nonlocal boundary layer vertical diffusion in a medium−range forecast model. *Mon. Wea. Rev.* **124**, 2322–2339.

Kanamitsu, M. 1975. On numerical prediction over a global tropical belt. Dept. of Meteorology Rep. 75-1, The Florida State University, Tallahassee.

Kanamitsu, M., Tada, K., Kudo, K., Sata, N. and Isa, S. 1983. Description of the JMA operational model. *J. Meteor. Soc. Japan* **61**, 812–828.

Kanamitsu, M. 1989. Description of the NMC global data assimilation and forecast system. *Wea. Forecast.* **4**, 335–342.

Kitade, T. 1983. Nonlinear normal mode initialization with physics. *Mon. Wea. Rev.* **111**, 2194–2213.

Krishnamurti, T. N., Xue, J., Bedi, H. S., Ingles, K. and Oosterhof, D. 1991. Physical initialization for numerical weather prediction over the tropics. *Tellus* **43AB**, 53–81.

Krishnamurti, T. N., Bedi, H. S. and Hardiker, V. M. 1998. *An Introduction to Global Spectral Modeling*. Oxford University Press, New York, 253 pp.

Krishnamurti, T. N., Kishtawal, C. M., LaRow, T., Bachiochi, D., Zhang, Z. and co-authors.1999. Improved weather and seasonal climate forecasts from multimodel superensemble. *Science* **285**, 1548–1550.

Krishnamurti, T. N., Kishtawal, C. M., Shin, D. W. and Williford, C. E. 2000a. Improving tropical precipitation forecasts from a multianalysis superensemble. *J. Climate* **13**, 4217–4227.

Krishnamurti, T. N., Kishtawal, C. M., Zhang, Z., LaRow, T., Bachiochi, D., and co-authors 2000b. Multimodel ensemble forecasts for weather and seasonal climate. *J. Climate* **13**, 4196–4216.

Krishnamurti, T. N., Surendran, S., Shin, D. W., Correa-Torres, R., Kumar, T. S. V., and co-authors 2001. Real Time Multianalysis/ Multimodel superensemble forecasts of precipitation using TRMM and SSM/I products. *Mon. Wea. Rev.* **129**, 2861–2883.

Krishnamurti, T. N. and Sanjay, J. 2003. A New Approach to the cumulus parameterization issue. *Tellus* **55A**, 275–300.

Krishnamurti, T. N., Gnanaseelan, C. and Chakraborty, A. 2007. Prediction of the diurnal change using a multimodel superensemble, Part I: precipitation. *Mon. Wea. Rev.,* in press.

Lacis, A. A. and Hansen, J. E. 1974. A parameterization for the absorption of solar radiation in the Earth's atmosphere. *J. Atmos. Sci.* **31**, 118–133.

Louis, J. F. 1979. A parametric model of vertical eddy fluxes in the atmosphere. *Bound.-Layer Meteor.* **17**, 187–202.

Manobianco, J. 1988. *On the Observational and Numerical Aspects of Explosive East Coast Cyclogenesis*. PhD Thesis, Department of Meteorology, Florida State University, USA, 361 pp.

O'Brien, J. J. 1970. A note on the vertical structure of the eddy exchange coefficients in the planetary boundary layer. *J. Atmos. Sci.* **27**, 1213–1215.

Pan, H.-L. and Wu, W.-S. 1995. *Implementing a mass flux convective parameterization package for the NMC Medium-Range Forecast model*. NMC Office Note 409, 40 pp.

Stull, R. B. 1988. *An Introduction to Boundary Layer Meteorology*. Kluwer Academic Publishers, Dordrecht. 666 pp.

Tiedke, M. 1984. The sensitivity of the time-mean large-scale flow to cumulus convection in the ECMWF model. *Proc. Workshop on Convection in Large-Scale Numerical Models*, Reading, Unitd Kingdom, ECMWF, 297–316.

Troen, I. and Mahrt, L. 1986. A simple model of the atmospheric boundary layer; sensitivity to surface evaporation. *Bound. –Layer Meteor.* **37**, 129–148.

Wallace, J. M., Tibaldi, S. and Simmons, A. J. 1983. Reduction of systematic forecast errors in the ECMWF model through the introduction of envelope orography. *Quart. J. Royal Meteor. Soc.* **109**, 683–718.

Yanai, M., Esbensen, S. and Chu, J.-H. 1973. Determination of bulk properties of tropical cloud clusters from large-scale heat and moisture budgets. *J. Atmos. Sci.* **30**, 611–627.